

Photonic Generation of Linearly Chirped Microwave Waveforms Using a Silicon-Based On-Chip Spectral Shaper Incorporating Two Linearly Chirped Waveguide Bragg Gratings

Weifeng Zhang, *Student Member, IEEE*, and Jianping Yao, *Fellow, IEEE, Fellow, OSA*

Abstract—Photonic generation of linearly chirped microwave waveforms using a silicon-based on-chip spectral shaper is proposed and demonstrated. The on-chip optical spectral shaper has a Mach–Zehnder interferometer (MZI) structure, in which two identical linearly chirped waveguide gratings (LC-WBGs) with opposite chirp rates are incorporated into the two arms. The LC-WBGs are fabricated on two rib waveguides by linearly varying the rib widths along the gratings to produce linear chirps. By adding an offset waveguide to one arm of the MZI and controlling the length of the offset waveguide, the spectral response of the shaper can be controlled to have a symmetrical, linearly increasing, or linearly decreasing free spectral range, which is needed for the generation of a linearly chirped microwave waveform based on spectral-shaping and wavelength-to-time mapping. The proposed device is fabricated using a CMOS-compatible process with 193-nm deep ultraviolet lithography. A theoretical analysis on the chirped microwave waveform generation is performed, which is verified by an experiment. Two linearly chirped microwave waveforms with symmetrical and uniform chirp profiles are experimentally generated using two fabricated spectral shapers with different lengths of the offset waveguides.

Index Terms—Chirped microwave waveform, linearly chirped waveguide grating, microwave photonics, optical pulse shaping, silicon photonics, wavelength-to-time mapping.

I. INTRODUCTION

IN modern radar systems, microwave pulse compression has been widely used to increase the range resolution [1]. Particularly, a linearly chirped microwave waveform (LCMW) with a large time-bandwidth product (TBWP) in the order of 10^2 or 10^3 , is highly preferred for microwave pulse compression [2]. An LCMW is usually generated electronically using a voltage-controlled electronic oscillator [3] or a digital waveform generator [4]. Due to the relatively low speed of electronic devices, electronically generated LCMWs are limited in the central frequency and bandwidth, usually less than a few to tens of gigahertz. However, for applications in advanced radar and wireless

Manuscript received July 27, 2015; revised October 12, 2015 and October 23, 2015; accepted October 23, 2015. Date of publication October 26, 2015; date of current version November 18, 2015. This work was supported in part by the Natural Sciences and Engineering Research Council of Canada through the Chicago Region Efficiency Environmental and Transportation Program and the CMC Microsystems of Canada.

The authors are with the Microwave Photonics Research Laboratory, School of Electrical Engineering and Computer Science, University of Ottawa, Ottawa, ON K1N 6N5, Canada (e-mail: jpyao@eecs.uottawa.ca).

Color versions of one or more of the figures in this paper are available online at <http://ieeexplore.ieee.org>.

Digital Object Identifier 10.1109/JLT.2015.2495105

systems, an LCMW with a central frequency up to tens or even hundreds of gigahertz and a bandwidth of a few gigahertz are often required [5]. To generate an LCMW with a high central frequency and wide bandwidth, a solution is to use photonics [6]–[9]. Thanks to the broad bandwidth inherent to photonics, an LCMW with a central frequency and bandwidth greater than tens of gigahertz can be generated. For example, by heterodyne-beating a continuous-wave optical signal with a pre-chirped optical pulse [8] or a chirped pulse from a fast wavelength-swept laser source [9] an LCMW can be generated. For example, in [9] an LCMW with a high frequency up to tens of GHz and an ultra-high TBWP up to 70 000 has been experimentally demonstrated. However, this approach requires two independent laser sources which would inevitably increase the system complexity and cost.

Due to the flexibility and simplicity, spectral-shaping and wavelength-to-time (SS-WTT) mapping has been considered one of the most important photonic-assisted solutions for arbitrary microwave waveform generation [10]–[12]. A typical SS-WTT mapping system consists of an ultra-short optical pulsed source, a spectral shaper, a dispersive element, and a photodetector (PD). The spectral shaper is the key device which is specifically designed to have a spectral response with a shape that is a scaled version of the microwave waveform to be generated. For LCMW generation, the spectral shaper usually has a spectral response with an increasing or decreasing free spectral range (FSR). By passing an ultra-short pulse (with a flat spectrum) through this spectral shaper, and allowing the spectrally shaped pulse to undergo WTT mapping in a dispersive element, an LCMW is generated at the output of a PD. Several approaches based on SS-WTT have been proposed recently to generate an LCMW [13]–[17]. In [13], a spectral shaper consisting of two superimposed linearly chirped fiber Bragg gratings (LC-FBGs) was proposed for LCMW generation. The generated LCMW has a central frequency of 15 GHz and a TBWP of 37.5. In [14], a single spatially discrete FBG acting as a spectral shaper was proposed and demonstrated for LCMW generation. The generated LCMW has a central frequency of 27.5 GHz and a TBWP of 16.8. A spectral shaper having a Mach–Zehnder interferometer (MZI) structure incorporating an optically pumped LC-FBG in one arm was also reported for LCMW generation [15]. The central frequency of the generated microwave waveform is about 39.54 GHz and a TBWP of 24.5. The major limitation of the approaches in [13]–[15] is the use of an FBG, which is highly

sensitive to environmental changes, thus the system stability is poor, or dedicated packaging must be made to increase the stability. In addition, the TBWPs are small which may not meet the requirements for practical applications. In [16] and [17], a spectral shaper was incorporated in one arm of an MZI with its function similar to an LC-FBG was proposed. An LCMW with a TBWP as large as 600 was generated. The stability was improved, but the size is very large and the cost is very high.

Recently, chip-level optical spectral shapers were proposed and demonstrated for LCMW generation [18]–[20]. In [18], a silicon-based spectral shaper consisting of multiple cascaded micro-ring resonators was proposed. By thermally tuning the rings, a spectral shaper with an increasing or decreasing FSR could be obtained. The generation of an LCMW with a central frequency of 8 GHz was demonstrated. However, due to the limited thermal-tuning range, the TBWP and the chirp rate of the generated LCMW were limited. To generate an LCMW with a large chirp rate, we have recently proposed and demonstrated a silicon-based on-chip optical spectral shaper [19]. The optical spectral shaper has an MZI structure in which multiple micro-ring resonators were cascaded. By controlling the radii of the micro-rings, the spectral response of the spectral shaper can be controlled to have a largely increasing or decreasing FSR. A largely chirped microwave waveform with a bandwidth of 15.55 GHz and a TBWP of 18.7 was demonstrated. The major limitation of this approach was the limited number of the micro-rings, making the TBWP of the generated LCMW still low. In [20], a silicon-based integrated distributed Fabry–Pérot cavity was used as a spectral shaper for the generation of an LCMW. Again, due to the limited group delay, the generated LCMW has a central frequency of 20 GHz and a small TBWP of 14.5.

Recently, we reported a novel silicon-based on-chip optical spectral shaper for the generation of an LCMW with a large TBWP [21]. The on-chip optical spectral shaper has an MZI structure that incorporates two identical linearly chirped waveguide gratings (LC-WBGs) with opposite chirp rates in the two arms. The LC-WBGs are fabricated on two rib waveguides and the chirps are realized by linearly varying the rib widths along the gratings. By adding an offset waveguide in one arm of the MZI and ensuring the length of the offset waveguide equal to length of LC-WBG, the spectral response of the spectral shaper was designed to have a linearly decreasing FSR, which was used in an experiment for generation of an LCMW with a large TBWP.

This paper is an extension of the work in [21] to study in more detail the operation of the waveform generation system using an on-chip spectral shaper, both theoretically and experimentally. Specifically, a theoretical analysis is performed to study the central frequency, chirp rate and the TBWP of the generated LCMWs based on the proposed spectral shaper. Then, the on-chip spectral shaper is fabricated and tested, and the use of the spectral shaper for LCMW generation is experimentally demonstrated. In the experiment, two spectral shapers with two different spectral responses having a symmetrical and a linearly decreasing FSR are used, which lead to the generation of LCMWs with symmetrical and uniform chirp profiles. The key advantage of the proposed on-chip spectral shaper is that two

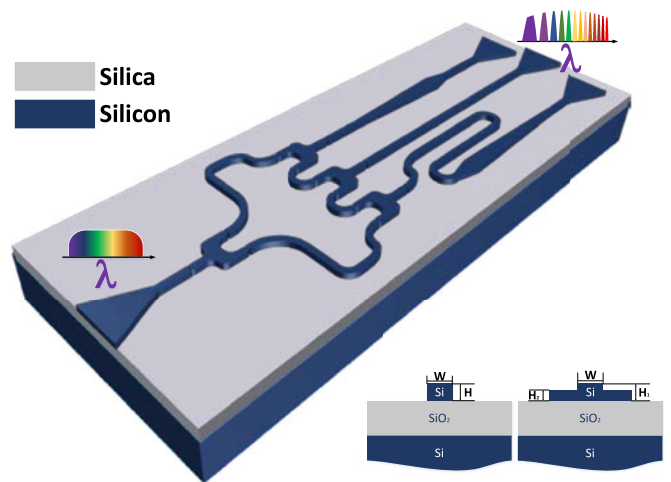


Fig. 1. Perspective view of the proposed on-chip silicon-based optical spectral shaper. (Inset: (left) Wire waveguide and (right) Rib waveguide).

identical LC-WBGs with opposite chirp rates in the two arms of the MZI are used which enables the system to generate an LCMW with a high chirp rate and a large TBWP. In addition, the use of the two LC-WBGs will also balance the losses of the two arms, thus making the spectral shaper with a spectral response having a high extinction ratio. Furthermore, the grating period of the LC-WBGs is uniform and the chirp rate is changed by varying the rib width, which is more robust than varying the grating period to achieve the chirp.

The proposed spectral shaper is fabricated using a CMOS compatible process with 193-nm deep ultraviolet lithography. The LC-WBGs are measured, each with a time delay of 228 ps and a bandwidth of 11 nm. By incorporating the LC-WBGs in a spectral shaper and using the spectral shaper in an SS-WTT mapping system, LCMWs are generated. Two spectral shapers are fabricated and used in the experiment. By using a spectral shaper with the length of the offset waveguide equal to zero, an LCMW having a symmetrical chirp profile is generated. The positive and negative chirp rates are, respectively, 5.4 and -4.9 GHz/ns, and the TBWP is 359.7. By using a spectral shaper with the length of the offset waveguide equal to the length of the LC-WBG, an LCMW having a uniform chirp profile is generated. The chirp rate is 1.54 GHz/ns and the TBWP is 615. This is the largest TBWP ever reported based on SS-WTT mapping technique, to the best of our knowledge.

II. DESIGN AND MEASUREMENT

Fig. 1 illustrates the perspective view of the proposed on-chip spectral shaper. The inset shows the fundamental structures of the strip waveguide and rib waveguide in the chip. To ensure a single transverse-electric (TE) mode operation, the strip waveguide is designed to have a width of 500 nm and a height of 220 nm, and the rib waveguide is designed to have a width of 500 nm, a height of 220 nm, and a slab thickness of 150 nm. Both waveguides are fabricated on top of a buried oxide layer (2 μm thick) on a silicon wafer. Fig. 2(a) presents the schematic layout of the proposed on-chip spectral shaper, which has an

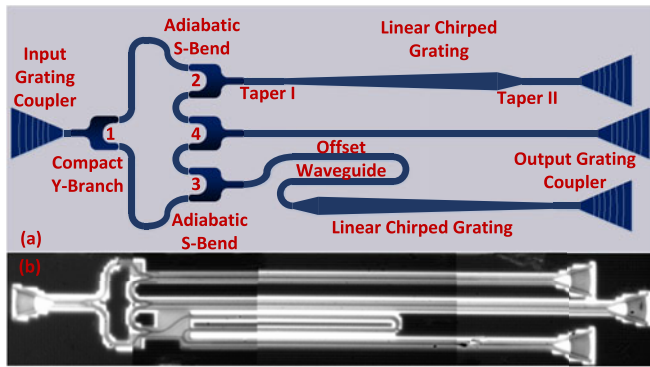


Fig. 2. (a) Schematic layout of the designed on-chip spectral shaper; (b) image of the fabricated spectral shaper with the length of the offset waveguide equal to the length of the LC-WBG captured by a microscope camera.

MZI structure that incorporates two identical LC-WBGs with opposite chirp rates in its two arms. Two TE-mode grating couplers [22] are employed to couple the light into or out of the chip. The input light is split by the first compact Y-branch [23] into two beams to travel through the LC-WBGs in the upper and lower arms. Spectral components of the light waves of different wavelengths are reflected from different positions in the LC-WBGs. By the second and third Y-branches, the reflected light waves are collected and recombined at the fourth Y-branch. The combined light wave is guided to the output grating coupler for coupling out of the chip. As a result of the optical interference at the recombination, the optical spectral shaper with a wavelength-dependent FSR is achieved. The FSR of the optical spectral shaper is defined here as the wavelength separation between two adjacent spectral peaks. To generate an LCMW based on the SS-WTT mapping technique, an increasing or decreasing FSR is usually required. In addition, an offset waveguide is added in the lower arm of the spectral shaper to control the length difference between the two arms which will lead to the change of the central frequency of the generated LCMW. By carefully designing the LC-WBGs and the length of the offset waveguide, the spectral response of the spectral shaper is controlled to have a symmetrical, a uniformly increasing or decreasing FSR. To minimize the chip footprint, the strip waveguide is mostly used to guide the light, and to reduce the bending loss, bend waveguides with a radius of $12 \mu\text{m}$ and adiabatic S-shape waveguide bends [24] are employed to direct the light. The rib waveguides are used in the implementation of the LC-WBG. Due to the different waveguide structures between the strip waveguide and the rib waveguide, a double-layer linear taper waveguide is required to achieve the mode transition. As shown in Fig. 2(a), there is a taper with a length of $50 \mu\text{m}$ at each of the two ends of the LC-WBGs. Note that at the right end of each of the LC-WBGs, a grating coupler is used as a waveguide terminator by irradiating the transmitted light to avoid reflection. Fig. 2(b) shows the image of the fabricated spectral shaper with the length of the offset waveguide equal to the length of the LC-WBG captured by a microscope camera.

The two LC-WBGs are the key components in the proposed on-chip spectral shaper. Fig. 3 shows the perspective view of

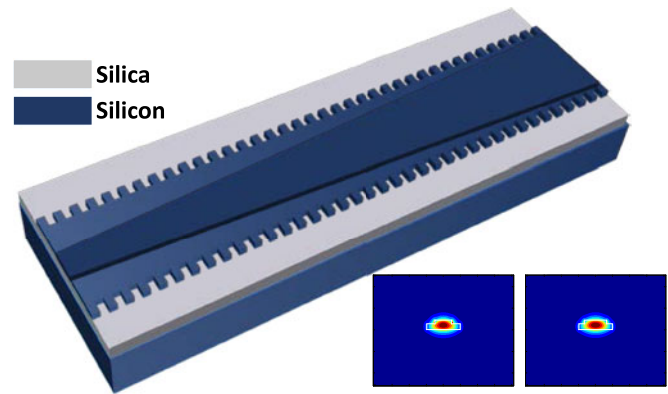


Fig. 3. Perspective view of the proposed LC-WBG. (Inset: Simulated fundamental TE mode profile of the rib waveguide with the rib width of 500 (left) and 650 nm (right)).

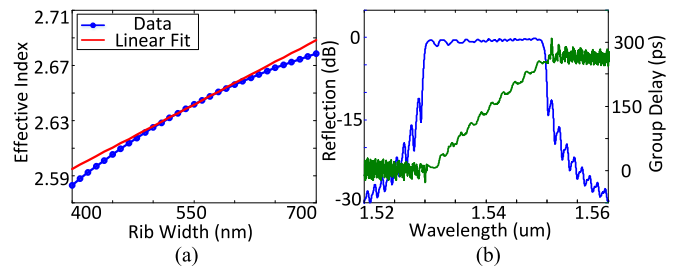


Fig. 4. (a) Effective refractive index for the fundamental TE mode in the rib waveguide at 1550 nm when the rib width is increasing. (b) Simulated spectral and group delay responses of the LC-WBG with the rib width increasing from 500 to 550 nm.

a designed LC-WBG. The grating is realized by introducing periodic sidewall corrugations on the slab. By keeping the grating period constant and linearly increasing the width of the rib along the grating, a linear chirp is produced since the effective refractive index is linearly increasing as the rib width increases. The inset in Fig. 3 shows the simulated fundamental TE mode profile in the rib waveguide with a rib width of 500 (left) and 650 nm (right). Fig. 4(a) shows the effective refractive index of the fundamental TE mode in the rib waveguide at 1550 nm as the rib width increases from 400 to 700 nm, as indicated in blue. The red curve gives the linear-fitting of the effective refractive index. As can be seen, the effective refractive index of the waveguide is linearly increasing, especially when the rib width increases from 500 to 590 nm. Thus, an LC-WBG is realized. The advantage of such an LC-WBG is that the grating period is uniform, which is more robust than varying the grating period to implement an LC-WBG [25]. To enable the LC-WBGs to work in the C band, the grating period is determined to be 300 nm with a duty cycle of 50%. The length of each of the LC-WBGs is 12.54 mm , to achieve a time delay of 223 ps. Fig. 4(b) shows the simulated reflection spectrum (blue) and the group delay (green) of the LC-WBG with the rib width increasing from 500 to 550 nm. The grating exhibits a time delay of 220 ps between 1530–1550 nm and thus has a dispersion value of 11 ps/nm and a chirp rate of 1.59 nm/mm. It is worth noting that the broad reflection bandwidth of the LC-WBG is due to the strong index

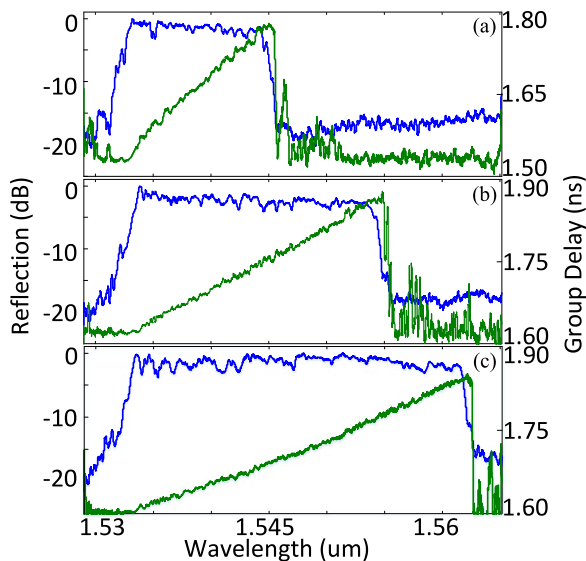


Fig. 5. Measured spectral and group delay responses of an LC-WBG with the rib width increasing from 500 to (a) 550, (b) 600, and (c) 650 nm.

modulation [26], which is much higher than that of a conventional LC-FBG.

The device is fabricated using a CMOS-compatible technology with 193-nm deep ultraviolet lithography at IMEC, Belgium, accessed via ePIXfab. The length of an LC-WBG is 12.54 mm and the entire on-chip spectral shaper incorporating two LC-WBGs has a size of 12.70 mm in length and 0.081 mm in width, giving a small footprint of 1.03 mm². First, the optical performance of the LC-WBGs is evaluated. The spectral and group delay responses of an LC-WBG are measured using an optical vector analyzer (LUNA OVA CTe). Fig. 5(a) shows the normalized reflection spectrum in blue and the group delay in green of an LC-WBG with the rib width linearly increasing from 500 to 550 nm. The grating exhibits a time delay of 228 ps between 1533–1544 nm and thus has a dispersion value of 20.7 ps/nm and a chirp rate of 0.88 nm/mm, which agree well with the simulated results in Fig. 4(b), except that the bandwidth becomes relatively smaller due to the inevitable fabrication imperfections [27]. Fig. 5(b) shows the normalized reflection spectrum and the group delay of an LC-WBG with the rib width linearly increasing from 500 to 600 nm. The grating exhibits a time delay of 236 ps between 1534–1554 nm and thus has a dispersion value of 11.8 ps/nm and a chirp rate of 1.59 nm/mm. Fig. 5(c) shows the normalized reflection spectrum and the group delay of an LC-WBG with the rib width linearly increasing from 500 to 650 nm. The grating exhibits a time delay of 241 ps between 1533–1562 nm and thus has a dispersion value of 8.3 ps/nm and a chirp rate of 2.31 nm/mm. As can be seen, it is easy to control the chirp rate of an LC-WBG by varying the rib width.

Then, the optical performance of the fabricated on-chip spectral shaper is evaluated. In the fabricated spectral shaper, the rib width of two LC-WBGs is varied from 500 to 550 nm. Fig. 6(a) shows the simulated spectral response of the on-chip spectral shaper with the length of the offset waveguide equal to

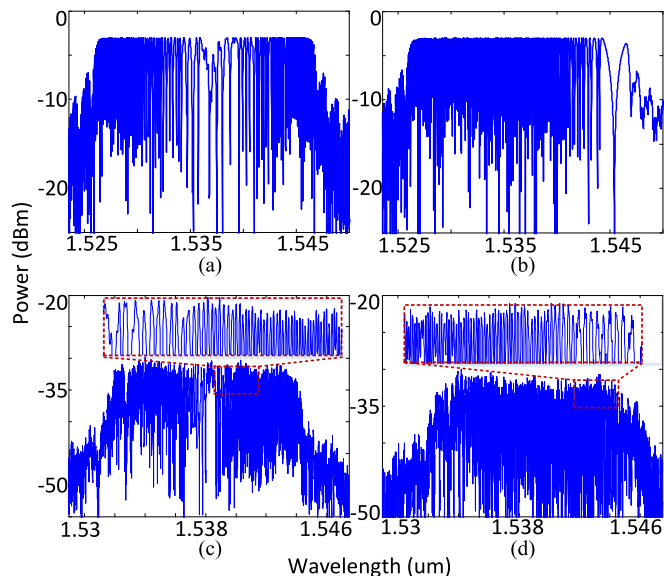


Fig. 6. Simulated spectral response of an on-chip spectral shaper when the length of the offset waveguide is equal to (a) zero, and (c) the length of the LC-WBG. Measured spectral response of a fabricated spectral shaper when the length of the offset waveguide is equal to (b) zero, and (d) the length of the LC-WBG.

zero. Since the length of the offset waveguide is zero, the spectral response presents a symmetrical FSR, and away from the center the FSR is linearly increasing. Fig. 6(b) shows the measured spectral response of the fabricated spectral shaper with the length of the offset waveguide equal to zero, and the inset shows the zoom-in view of part of the spectral response. As can be seen, the spectral response agrees well with that shown in Fig. 6(a) except the different bandwidths caused by the fabrication imperfections. Fig. 6(c) shows the simulated spectral response of the on-chip spectral shaper, in which the length of the offset waveguide is set to be equal to the length of the LC-WBG. Note that due to the waveguide structure difference between the offset waveguide and the LC-WBG waveguide, the lengths are the effective lengths. The spectral response presents a linearly decreasing FSR. Fig. 6(d) shows the measured spectral response of the fabricated spectral shaper with the length of the offset waveguide equal to the length of the LC-WBG and the inset shows the zoom-in view of part of spectral response. Again, the spectral response agrees well with that shown in Fig. 6(c) except the different bandwidth caused by the fabrication imperfections. It is worth noting that the measured spectral responses show a reduced modulation depth, which is mainly caused by the limited resolution of the optical vector analyzer. In addition, the insertion loss of the fabricated spectral shaper is measured to be around 30 dB, which is mainly resulted from the fiber-to-fiber coupling loss and the splitting loss at the Y-branch. To ensure a full view of the spectrums, the different wavelength ranges on the x-axis are used in Fig. 6.

III. PRINCIPLE

The fundamental principle of the SS-WTT mapping technique is illustrated in Fig. 7. An ultrashort optical pulse emitted

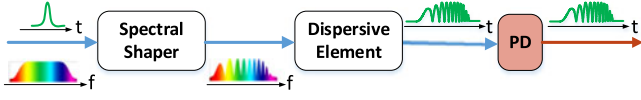


Fig. 7. Schematic of a microwave waveform generation system based on SS-WTT mapping technique.

from a mode-locked laser is first spectrally shaped by the on-chip optical spectral shaper. Then, the spectrum-shaped optical pulse is sent to a dispersive element to perform linear WTT mapping. At the output of a high-speed PD, a microwave waveform with the shape identical to that of the shaped optical spectrum is generated.

Mathematically, the on-chip spectral shaper incorporating two identical LC-WBGs with the opposite chirp rates can be modeled as a two-tap delay-line filter. The transfer function of the spectral shaper is given by

$$T(\lambda) = \frac{1}{2}W(\lambda) \left[1 + \cos\left(\frac{2\pi n_{eff}}{\lambda} 2\Delta L\right) \right], \quad (1)$$

$$\left(|\lambda - \lambda_0| \leq \frac{B_\lambda}{2} \right)$$

where $W(\lambda)$ is the intensity reflection spectrum of the LC-WBG, B_λ is the bandwidth of the spectral shaper where we assume that the input ultra-short pulse has a spectral width that is wider than the bandwidth of the spectral shaper, n_{eff} is the effective refractive index of the waveguide, and ΔL is the length difference between the two arms of the MZI in the spectral shaper, which includes the wavelength-independent path difference ΔL_0 caused by the offset waveguide (since the length of the offset waveguide is small, the dispersion can be ignored), and the wavelength-dependent length difference introduced by the chirp of the LC-WBG $\Delta L_1(\lambda)$. ΔL_0 can be controlled by selecting the length of the offset waveguide, and $\Delta L_1(\lambda)$ is determined by the bandwidth and the chirp rate of the LC-WBG, which can be calculated using $\Delta L_1(\lambda) = \delta\lambda/C$, where $\delta\lambda$ (nm) is the wavelength detuning from the center wavelength λ_0 , and C (nm/mm) is the chirp rate of the LC-WBG. Note that $\delta\lambda$ is positive when the reflection position is at shorter wavelength than λ_0 , and $\delta\lambda$ is negative when the reflection position is at longer wavelength than λ_0 . Then, the transfer function $T(\lambda)$ can be rewritten as

$$T(\lambda) = \frac{1}{2}W(\lambda) \left\{ 1 + \cos\left[\frac{2\pi}{\lambda} (2n_{eff0}\Delta L_0 + 2 \cdot n_{eff1}\Delta L_1)\right] \right\} \quad (2)$$

where n_{eff0} is the effective refractive index of the strip waveguide and n_{eff1} is the average effective refractive index of the rib waveguide along the grating. At 1550 nm, the effective refractive index of the strip waveguide for the fundamental TE mode is calculated to be 2.379, and the effective refractive index of the rib waveguide is calculated to be 2.627. It is worth noting that since a pair of LC-WBGs with opposite chirp rates are incorporated in the two arms of the MZI, the wavelength-dependent length difference introduced by ΔL_1 is doubled, which also

leads to the doubling in the chirp rate, and thus the TBWP of the generated microwave waveform.

The spectral response presents a varying FSR due to the chirp of the LC-WBGs. The FSR of the optical spectral shaper response is a function of wavelength and can be expressed as

$$FSR = \frac{\lambda^2}{2n_{eff}\Delta L} \cong \frac{\lambda_0^2}{2(n_{eff0}\Delta L_0 + 2n_{eff1}\frac{\delta\lambda}{C})}. \quad (3)$$

According to (3), by properly selecting the parameters of the LC-WBGs and controlling the length of the offset waveguide, the FSR of the optical spectral shaper can be specifically controlled to be systematical, linearly increasing or decreasing.

The spectrum-shaped optical pulse is then sent to the dispersive element and the shaped spectrum is mapped to a temporal microwave waveform thanks to the dispersion-induced linear WTT mapping, and then detected by the high-speed PD. According to the mapping relationship in [8], the converted time-domain microwave waveform is given by

$$y(t) \propto \frac{1}{2}W\left(\frac{t}{\ddot{\Phi}_\lambda}\right) \left\{ 1 + \cos\left[\frac{4\pi}{\lambda_0^2} \times \frac{t}{\ddot{\Phi}_\lambda} \left(n_{eff0}\Delta L_0 + 2n_{eff1}\frac{\delta t}{C\ddot{\Phi}_\lambda}\right)\right] \right\} \quad (4)$$

where δt is the time detuning from the center of the temporal waveform, which is given by the mapping relationship $\delta\lambda \rightarrow \delta t/\ddot{\Phi}_\lambda$, and $\ddot{\Phi}_\lambda$ is the group velocity dispersion (GVD) of the dispersive element. The time-domain duration of the generated microwave waveform is determined by the window function $W(t/\ddot{\Phi}_\lambda)$ and is calculated by $\Delta T = B_\lambda\ddot{\Phi}_\lambda$.

The instantaneous microwave frequency of the generated waveform can be obtained from the phase term of (4), which is given by

$$f_{RF}(\delta t) = \frac{1}{2\pi} \times \frac{d\Psi}{dt} = \frac{2}{\lambda_0^2} \times \frac{n_{eff0}\Delta L_0}{\ddot{\Phi}_\lambda} \pm \frac{4}{\lambda_0^2} \times \frac{n_{eff1}\delta t}{C\ddot{\Phi}_\lambda^2}. \quad (5)$$

As can be seen the generated microwave waveform is linearly chirped. For a given dispersive element, the central frequency of the generated chirped microwave waveform is given by

$$f_{RF}(\delta t = 0) = \frac{1}{2\pi} \times \frac{d\Psi}{dt} = \frac{2}{\lambda_0^2} \times \frac{n_{eff0}\Delta L_0}{\ddot{\Phi}_\lambda} \quad (6)$$

which is only determined by the length of the offset waveguide. Thus, LCMWs with different chirp profiles (symmetrical and uniform) can be generated by simply tuning ΔL_0 .

The chirp rate of the generated microwave waveform, given by

$$CR = \frac{df_{RF}(\delta t)}{dt} = \pm \frac{4}{\lambda_0^2} \times \frac{n_{eff1}}{C\ddot{\Phi}_\lambda^2} \quad (7)$$

which is dependent on the chirp rate of the LC-WBG and the GVD of the dispersive element. A positive or negative chirp rate corresponds to a positive and negative value of ΔL_0 , respectively. By carefully designing the length of the offset waveguide and choosing the chirp rate of the LC-WBG, an LCMW with required chirp profile can be generated.

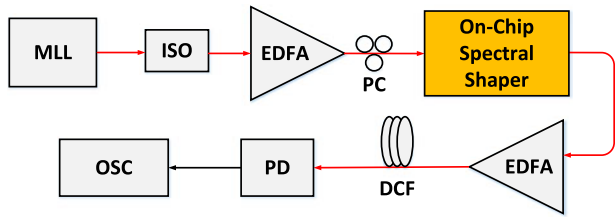


Fig. 8. Experimental setup. MML: mode lock laser. ISO: isolator; EDFA: erbium-doped fiber amplifier. PC: polarization controller. DCF: dispersion compensating fiber. PD: photodetector. OSC: oscilloscope.

The pulse compression ratio is determined by the TBWP of the transmitted microwave waveform. In our system, the TBWP of the generated LCMW is given by

$$TBWP = CR \times \Delta T^2 = \frac{4}{\lambda_0^2} \times \frac{n_{eff} l}{C} B_\lambda^2. \quad (8)$$

It is shown that the TBWP is independent of the GVD of the dispersive element in the system but is determined by the chirp rate and the bandwidth of the LC-WBGs.

IV. EXPERIMENT

Fig. 8 shows the experimental setup. An optical Gaussian pulse train generated by a mode-lock laser (Pritel 1550-nm Picosecond and Femtosecond Fiber Lasers) with a pulse duration of approximately 600 fs and a repetition rate of 40 MHz is sent to the on-chip spectral shaper via an isolator and after amplification by an EDFA. The spectral width of an optical pulse in the pulse train is 12 nm, which is wider than the bandwidth of the spectral shaper. The EDFA is used to increase the power of the optical pulse. A polarization controller is connected between the EDFA and the spectral shaper to adjust the state of polarization of the input signal to minimize the polarization-dependent loss. After SS by the spectral shaper, a spectrally-shaped optical pulse is obtained which is first amplified by a second EDFA and then sent to a dispersion compensating fiber (DCF) serving as a dispersive element to perform WTT mapping. The optical intensity envelope is then converted to a microwave signal at a PD with a bandwidth of 45 GHz (NewFocus Model 1014), and the generated time-domain microwave signal is monitored using a sampling oscilloscope with a bandwidth of 63 GHz (OSC, Agilent 86116A).

First, an on-chip spectral shaper with the length of the offset waveguide equal to zero is incorporated into the SS-WTT mapping system to generate an LCMW with a symmetrical chirp profile. An ultra-short optical pulse is spectrum shaped by the spectral shaper, and is then sent to the DCF (with a GVD of -1020 ps/nm) to perform WTT mapping to generate a chirped microwave waveform. As shown in Fig. 9(a), an LCMW with a symmetrical chirp profile is generated. The pulse duration is around 10.90 ns. The spectrogram of the generated LCMW is calculated and is shown in Fig. 9(b). Here the spectrogram is calculated by applying a Hamming window with a width of 1.3 ns to divide the waveform into sections. Then, the short-time Fourier transform is applied to estimate the spectrum. As

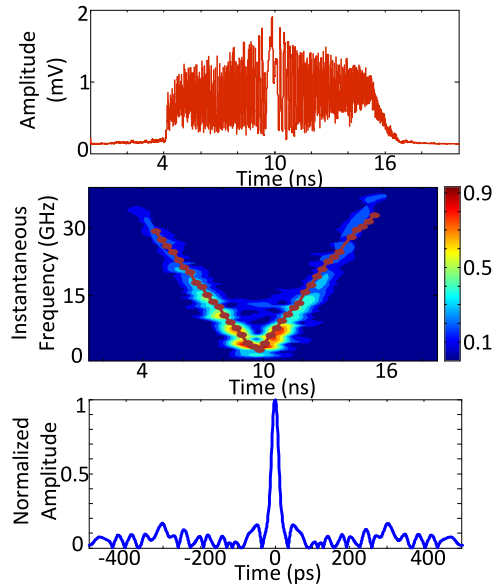


Fig. 9. Experimental results. (a) The generated LCMW; (b) the spectrogram and instantaneous frequency of the generated LCMW, and (c) the compressed pulse by autocorrelation.

can be seen, the waveform is chirped with a symmetrical chirp profile. To further confirm the chirp of the waveform, the instantaneous microwave frequency based on Hilbert transform is also calculated [28] and given by the red-dotted line in Fig. 9(b), which agrees well with the spectrogram. The central frequency of the generated symmetrically chirped microwave waveform is 1.2 GHz, which is different from the theoretical prediction of 0 GHz according to (6). Such a difference is due to a small asymmetry between the two arms of the MZI in the spectral shaper, which is caused by fabrication imperfections. On the right side of the center, the instantaneous frequency is linearly increasing with a positive chirp rate of 5.4 GHz/ns, which agrees quite well with the theoretical predictions of 4.8 GHz/ns by (7). On the left side of the center, the instantaneous frequency is linearly decreasing with a negative chirp rate of -4.9 GHz/ns. The small difference in the chirp rates is resulted from a small asymmetry of the two LC-WBGs in the two arms of the MZI, which is also caused by fabrication imperfections. According to the time-domain waveform and its carrier frequency distribution, the TBWP of the generated LCMW is estimated to be around 359.7. Fig. 9(c) shows the compressed pulse with a pulse width of 24 ps, which is obtained by calculating the autocorrelation of the generated microwave waveform. Note that before calculating the autocorrelation, the direct-current component in the generated LCMW is filtered out. By comparing the pulse width of the waveforms in Fig. 9(a) and (c), a pulse compression ratio as large as 454.2 is obtained.

Then, a second on-chip spectral shaper with the length of the offset waveguide equal to the length of the LC-WBG is incorporated into the SS-WTT mapping system to generate an LCMW with a linearly increasing chirp. Note that the input optical pulse is the same as the one in the first experiment. The spectrum-shaped optical pulse is then sent to the DCF (with a

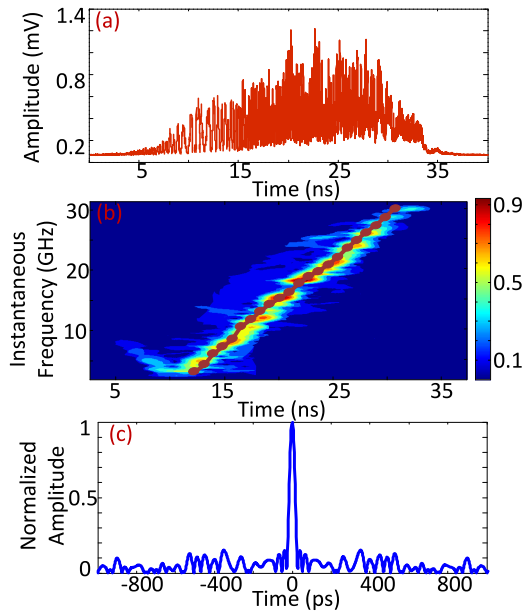


Fig. 10. Experimental results. (a) The generated LCMW, (b) the spectrogram and instantaneous frequency of the generated LCMW, and (c) the compressed pulse.

GVD of -1700 ps/nm) where the spectrum is mapped to the time domain to generate a chirped microwave waveform. As shown in Fig. 10(a), an LCMW with a linearly increasing chirp is generated. The pulse duration is around 20.5 ns. Fig. 10(b) shows the spectrogram plot of the generated LCMW. To further confirm the linear chirp, the instantaneous microwave frequency is given by the red-dotted line. Again, the results agree well with the spectrogram. The center frequency of the generated LCMW is 15.8 GHz, which agrees well with the theoretical prediction of 16.4 GHz according to (6). The LCMW has a positive chirp rate of 1.54 GHz/ns, which also agrees well with the theoretical prediction of 1.42 GHz/ns by (7). According to the time-domain waveform and its carrier frequency distribution, the TBWP of the generated LCMW is estimated to be around 615, which also agrees well with the theoretically predicted TBWP of 612.5 by (8). Fig. 10(c) shows the compressed pulse with a pulse width of 32.9 ps, which is obtained by calculating the autocorrelation of the generated microwave waveform. By comparing the pulse width of the waveforms in Fig. 10(a) and (c), a pulse compression ratio as large as 623.1 is obtained.

The two generated LCMWs shown in Figs. 9 and 10 have different chirp rates, since the dispersive element (DCF) for WTT mapping has a different GVD. In addition, to further increase the TBWP, we may increase the rib widths along the gratings to increase the reflection bandwidths of the LC-WBGs. Thus, the spectral shaper could have a wider bandwidth. However, it is worth noting that in the theoretical analysis we assume that the input ultra-short pulse has a wider spectral width than the bandwidth of the spectral shaper, and B_λ is determined to be the bandwidths of the LC-WBGs. In fact, when the bandwidth of the spectral shaper is wider than the spectral width of the input ultra-short pulse, B_λ would be smaller, and is determined by the spectral width of the input ultra-short pulse.

V. DISCUSSION AND CONCLUSION

In the experiment, the WTT mapping was done using a DCF serving as the dispersive element. In fact, the DCF can be replaced by an LC-WBG if the GVD of the LC-WBG is large enough. In this case, it is feasible to integrate an optical spectral shaper and a dispersive element on a single chip, which would make the system much smaller. To have an LC-WBG with a large GVD, the length should be very long, which would increase the footprint. This is the difficulty imposed on the use of an LC-WBG for WTT mapping. A possible solution is to have an LC-WBG with a spiral layout to maximize the use of the chip area.

In conclusion, photonic generation of LCMWs with a large TBWP using a silicon-based on-chip spectral shaper in an SS-WTT mapping system was proposed and demonstrated. The key component in the SS-WTT mapping system was an on-chip optical spectral shaper, which was designed to have an MZI structure incorporating two identical LC-WBGs with opposite chirp rates in its two arms. The LC-WBGs were fabricated on two rib waveguides and the frequency chirp was realized by linearly varying the rib widths along the gratings. By adding an offset waveguide in one arm of the MZI and controlling the length of the offset waveguide, the spectral response of the spectral shaper could be controlled to have a symmetrical, a linearly increasing or linearly decreasing FSR. Through SS using the on-chip spectral shaper and WTT mapping using a dispersive element, an LCMW could be generated. Two spectral shapers with two different lengths of the offset waveguides were fabricated and applied in the experiment to generate two LCMWs with different chirp profiles. Using an on-chip spectral shaper with a length of the offset waveguide equal to zero, an LCMW with a symmetrical chirp profile was generated, which had a chirp rate of 5.4 and -4.9 GHz/ns for the positive and negative portion of the waveform, respectively, and a TBWP of 359.7. Using an on-chip spectral shaper with the length of the offset waveguide equal to the length of the LC-WBG, an LCMW with a uniform chirp profile was generated, which had a chirp rate of 1.54 GHz/ns and a TBWP of 615. This TBWP is the highest value ever reported using SS-WTT mapping technique. The key feature of the proposed approach was LCMWs with a large chirp rate and the TBWP could be generated thanks to the use of an on-chip spectral shaper incorporating a pair of LC-WBGs with opposite chirp rates.

ACKNOWLEDGMENT

The author would like to thank CMC Microsystems, for providing the design tools and enabling the fabrication of the device.

REFERENCES

- [1] D. K. Barton, *Radar System Analysis Modeling*. Boston, MA, USA: Artech House, 2005.
- [2] A. W. Rihaczek, *Principles High-Resolution Radar*. Norwood, MA, USA: Artech House, 1996.
- [3] H. D. Griffiths and W. J. Bradford, "Digital generation of high time bandwidth product linear FM waveforms for radar altimeters," *Proc. IEE-F*, vol. 139, no. 2, pp. 160–169, Apr. 1992.

- [4] H. Kwon and B. Kang, "Linear frequency modulation of voltage controlled oscillator using delay-line feedback," *IEEE Microw. Wireless Compon. Lett.*, vol. 15, no. 6, pp. 431–433, Jun. 2005.
- [5] D. T. Petkie, C. Benton, and E. Bryan, "Millimeter wave radar for remote measurement of vital signs," in *Proc. IEEE Radar Conf.*, May 2009, pp. 1–3.
- [6] A. Zeitouny, S. Stepanov, O. Levinson, and M. Horowitz, "Optical generation of linearly chirped microwave pulses using fiber Bragg gratings," *IEEE Photon. Technol. Lett.*, vol. 17, no. 3, pp. 660–662, Mar. 2005.
- [7] Y. Dai and J. P. Yao, "Chirped microwave pulse generation using a photonic microwave delay-line filter with a quadratic phase response," *IEEE Photon. Technol. Lett.*, vol. 21, no. 9, pp. 569–571, May 2009.
- [8] H. Gao, C. Lei, M. Chen, F. Xing, H. Chen, and S. Xie, "A simple photonic generation of linearly chirped microwave pulse with large time-bandwidth product and high compression ratio," *Opt. Exp.*, vol. 21, no. 20, pp. 23107–23115, Oct. 2013.
- [9] J.-W. Shi, F.-M. Kuo, N.-W. Chen, S. Y. Set, C.-B. Huang, and J. E. Bowers, "Photonic generation and wireless transmission of linearly/nonlinearly continuously tunable chirped millimeter-wave waveforms with high time-bandwidth product at W-band," *IEEE Photon. J.*, vol. 4, no. 1, pp. 215–223, Feb. 2012.
- [10] J. P. Yao, "Photonic generation of microwave arbitrary waveforms," *Opt. Commun.*, vol. 284, no. 15, pp. 3723–3736, Jul. 2011.
- [11] L. R. Chen, "Photonic generation of chirped microwave and millimeter wave pulses based on optical spectral shaping and wavelength-to-time mapping in silicon photonics," *Opt. Commun.*, 2015, DOI: 10.1016/j.optcom.2015.04.023.
- [12] V. Torres Company, D. E. Leaird, and A. M. Weiner, "Dispersion requirements in coherent frequency-to-time mapping," *Opt. Exp.*, vol. 19, no. 24, pp. 24718–24729, Nov. 2011.
- [13] C. Wang and J. P. Yao, "Photonic generation of chirped microwave pulses using superimposed chirped fiber Bragg gratings," *IEEE Photon. Technol. Lett.*, vol. 20, no. 11, pp. 882–884, Jun. 2008.
- [14] C. Wang and J. P. Yao, "Large time-bandwidth product microwave arbitrary waveform generation using a spatially discrete chirped fiber Bragg grating," *J. Lightw. Technol.*, vol. 28, no. 11, pp. 1652–1660, Jun. 2010.
- [15] R. Ashrafi, Y. Park, and J. Azana, "Fiber-based photonic generation of high-frequency microwave pulses with reconfigurable linear chirp control," *IEEE Trans. Microw. Theory Technol.*, vol. 58, no. 11, pp. 3312–3319, Nov. 2010.
- [16] A. Rashidinejad and A. M. Weiner, "Photonic radio-frequency arbitrary waveform generation with maximal time-bandwidth product capability," *J. Lightw. Technol.*, vol. 32, no. 20, pp. 3383–3393, Oct. 2014.
- [17] Y. Li, A. Rashidinejad, J.-M. Wun, D. E. Leaird, J.-W. Shi, and A. M. Weiner, "Photonic generation of W-band arbitrary waveforms with high time-bandwidth products enabling 3.9 mm range resolution," *Optica*, vol. 6, no. 1, pp. 446–454, Dec. 2014.
- [18] M. Khan, H. Shen, Y. Xuan, L. Zhao, S. Xiao, D. E. Leaird, A. M. Weiner, and M. Qi, "Ultrabroad-bandwidth arbitrary radiofrequency waveform generation with a silicon photonic chip-based spectral shaper," *Nature Photon.*, vol. 4, no. 2, pp. 117–122, Feb. 2010.
- [19] W. Zhang, J. Zhang, and J. P. Yao, "Largely chirped microwave waveform generation using a silicon-based on-chip optical spectral shaper," presented at the Int. Topical Meet. Microwave Photonics/9th Asia-Pacific Microwave Photonics Conf., Sapporo, Japan, Oct. 20–23, 2014.
- [20] M. Ma, M. Rochette, and L. R. Chen, "Generating chirped microwave pulses using an integrated distributed Fabry-Pérot cavity in silicon-on-insulator," *IEEE Photon. J.*, vol. 7, no. 2, art. no. 5500706, Apr. 2015.
- [21] W. Zhang and J. P. Yao, "Photonic generation of linearly chirped microwave waveform with a large time-bandwidth product using a silicon-based on-chip spectral shaper," presented at the Int. Topical Meet. Microwave Photonics, Paphos, Cyprus, Oct. 26–29, 2015.
- [22] Y. Wang, J. Flueckiger, C. Lin, and L. Chrostowski, "Universal grating coupler design," *Proc. SPIE*, vol. 8915, p. 89150Y, May 2013.
- [23] Y. Zhang, S. Yang, A. E.-J. Lim, G.-Q. Lo, C. Galland, T. Baehr-Jones, and M. Hochberg, "A compact and low loss Y-junction for submicron silicon waveguide," *Opt. Exp.*, vol. 21, no. 1, pp. 1310–1316, Jan. 2013.
- [24] W. Bogaerts and S. K. Selvaraja, "Compact single-mode silicon hybrid rib/strip waveguide with adiabatic bends," *IEEE Photon. J.*, vol. 3, no. 3, pp. 422–432, Jun. 2011.
- [25] M. Spasojevic and L. R. Chen, "Discretely tunable optical delay lines using serial and step-chirped sidewall Bragg gratings in SOI," *Electron. Lett.*, vol. 49, no. 9, pp. 608–610, Apr. 2013.
- [26] X. Wang, W. Shi, R. Vafaei, N. Jaeger, and L. Chrostowski, "Uniform and sampled Bragg gratings in SOI strip waveguides with sidewall corrugations," *IEEE Photon. Technol. Lett.*, vol. 23, no. 5, pp. 290–292, Mar. 2011.
- [27] X. Wang, W. Shi, H. Yun, S. Grist, N. A. F. Jaeger, and L. Chrostowski, "Narrow-band waveguide Bragg gratings on SOI wafers with CMOS-compatible fabrication process," *Opt. Exp.*, vol. 20, no. 14, pp. 15547–15558, Jun. 2012.
- [28] S. Mallet, *A Wavelet Tour Signal Processing*. San Diego, CA, USA: Academic, 1999.

Weifeng Zhang (S'12) received the B.Eng. degree in electronic science and technology from Xi'an Jiaotong University, Xi'an, China, in 2008, and the M.A.Sc. degree in electrical engineering from the Polytechnic University of Turin, Turin, Italy, in 2011. He is currently working toward the Ph.D. degree at the Microwave Photonics Research Laboratory, School of Electrical Engineering and Computer Science, University of Ottawa, Ottawa, ON, Canada.

His current research interests include silicon photonics and its applications in microwave photonics.

Jianping Yao (M'99–SM'01–F'12) received the Ph.D. degree in electrical engineering from the Université de Toulon, Toulon, France, in December 1997. He is a Professor and the University Research Chair in the School of Electrical Engineering and Computer Science, University of Ottawa, Ottawa, ON, Canada. He was an Assistant Professor with the School of Electrical and Electronic Engineering, Nanyang Technological University, Singapore, in 1998. In December 2001, He joined the School of Electrical Engineering and Computer Science, University of Ottawa, as an Assistant Professor, where he became an Associate Professor in 2003, and a Full Professor in 2006. He was the University Research Chair in Microwave Photonics in 2007. From July 2007 to June 2010, He was the Director of the Ottawa-Carleton Institute for Electrical and Computer Engineering and was reappointed Director of the Ottawa-Carleton Institute for Electrical and Computer Engineering in 2013. He has published more than 500 papers, including more than 290 papers in peer-reviewed journals and 210 papers in conference proceedings.

Dr. Yao was a Guest Editor for the Focus Issue on Microwave Photonics in *Optics Express* in 2013 and a Feature Issue on Microwave Photonics in *Photonics Research* in 2014. He is currently a Topical Editor for *Optics Letters*, and serves on the Editorial Board of the IEEE TRANSACTIONS ON MICROWAVE THEORY AND TECHNIQUES, *Optics Communications*, and *China Science Bulletin*. He is a Chair of numerous international conferences, symposia, and workshops, including the Vice Technical Program Committee (TPC) Chair of the IEEE Microwave Photonics Conference in 2007, TPC Cochair of the Asia-Pacific Microwave Photonics Conference in 2009 and 2010, TPC Chair of the high-speed and broadband wireless technologies subcommittee of the IEEE Radio Wireless Symposium in 2009–2012, TPC Chair of the microwave photonics subcommittee of the IEEE Photonics Society Annual Meeting in 2009, TPC Chair of the IEEE Microwave Photonics Conference in 2010, General Cochair of the IEEE Microwave Photonics Conference in 2011, TPC Cochair of the IEEE Microwave Photonics Conference in 2014, and General Cochair of the IEEE Microwave Photonics Conference in 2015. He received the 2005 International Creative Research Award at the University of Ottawa. He received the 2007 George S. Glinski Award for Excellence in Research and was selected to receive an inaugural OSA outstanding reviewer award in 2012. He is an IEEE MTT-S Distinguished Microwave Lecturer for 2013–2015. He is a registered Professional Engineer of Ontario. He is a Fellow of the Optical Society of America and the Canadian Academy of Engineering.